ACS APPLIED ENERGY MATERIALS

www.acsaem.org Article

Effects of F and Cl Doping in Cubic $Li_7La_3Zr_2O_{12}$ Solid Electrolyte: A First-Principles Investigation

Yu Yang and Hong Zhu*

Cite This: ACS Appl. Energy Mater. 2022, 5, 15086−15092 Read Online

ACCESS | Metrics & More | Article Recommendations | Supporting Information

ABSTRACT: Anion doping is recently attaining a lot of research interest for solid-state electrolytes. In this study, we investigated the effects of F and Cl on the phase, electrochemical, and chemical stabilities; ionic conductivity; and diffusion mechanism in cubic $Li_7La_3Zr_2O_{12}$ (c-LLZO), based on density functional theory (DFT) calculations. It is found that a homogeneous diffusion network with low local structural distortion and the high Li jump numbers are beneficial for good ionic conductivity in c-LLZO. The introduction of a certain amount of Li vacancies can enhance both the Li jump numbers and the concerted migration percentage of c-LLZO. Our findings deepen the understanding of the diffusion mechanism in c-LLZO and offer a valuable insight for the rational design of solid electrolytes.

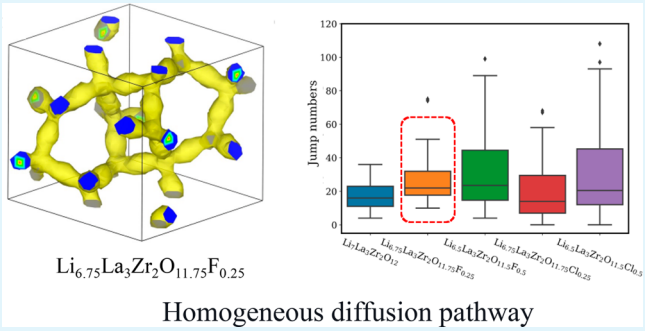

KEYWORDS: *garnets, density functional theory, ab initio molecular dynamics, solid electrolyte, lithium ionic conductivity*

Downloaded via SHANGHAI JIAO TONG UNIV on January 4, 2023 at 04:18:13 (UTC).
See https://pubs.acs.org/sharingguidelines for options on how to legitimately share published articles.

■ INTRODUCTION

All-solid-state lithium ion batteries (ASSLIBs) with solid-state electrolytes (SSEs) are the next-generation of battery technology due to its potential advantages in safety and performance.[1,2] Among various solid-state electrolyte materials, garnet-structured electrolytes have received a lot of attention because of their high ionic conductivity and excellent stability vs Li metal.[3] The composition of garnet electrolytes is $Li_{3+x}A_3B_2O_{12}$, where A and B are various cations, coordinated by eight and six oxygen atoms, respectively, and x varies based on the charge balance.[4,5] Among garnet electrolytes, the $Li_7La_3Zr_2O_{12}$ (LLZO) crystallizes in the tetragonal phase (t-LLZO) at room temperature and transforms to the cubic phase (c-LLZO) at 800−1000 K.[6] The t-LLZO with an ordered Li sublattice exhibits poor ionic conductivity (around 10^{-6} S cm^{-1}), while c-LLZO shows high ionic conductivity on the order of 10^{-4} S cm^{-1},[6] due to the disordered Li sublattice (all Li sites are partially occupied).[6] Meier et al. have revealed that, in t-LLZO, the ordered Li sublattice results in synchronous collective motions of Li ions, which requires higher activation energy. But in c-LLZO, the asynchronous mechanism of the single-ion jumping induced the collective motion of Li ions with lower activation energies.[7]

Cation doping is a common method to stabilize c-LLZO at room temperature and improve the ionic conductivity of c-LLZO. There are three doping sites in c-LLZO, namely, Li site, La site, and Zr site, respectively. The high valent cation doping can introduce lithium ion vacancies, increase the disorder of the lithium ion lattice, decrease the phase transition temperature, and stabilize the cubic phase at room temperature.[6,8] The common doping elements at Li sites are Al, Ga, and Fe. Daniel Rettenwander reported that Al and Ga codoping improved the ionic conductivity of c-LLZO to 1.2×10^{-3} S cm^{-1}.[9] The La site is considered to have a great impact on the crystal structure of c-LLZO, determining the size of the bottleneck for Li transport.[10] Ezhiylmurugan Rangasamy first doped Ce at the La site in *c*-LLZO, which enhanced the Li vacancies and improved the ionic conductivity.[11] The doping at Zr sites has been widely studied, and the common doping elements include Ta,[12] Te,[13] and Nb.[14] These doping elements do not affect the distribution of Li^+ after entering the lattice, without hindering the transport of Li^+.[10] Since the anion sublattices have a critical influence on the ionic conductivity of solid-state Li ion conductors,[15] anion doping and substitution are gaining more and more research momentum.[16−19] For the c-LLZO system, the experimenters have prepared F-doped LLZO in the cubic phase, exhibiting a conductivity of 5×10^{-4} S cm^{-1} and an activation energy of 0.26 eV.[20] Further, computational researchers have used classical molecular dynamics methods to confirm that fluoride ions are likely to remain on the oxygen sites, the F-doped LLZO

Received: August 27, 2022
Accepted: November 7, 2022
Published: November 16, 2022

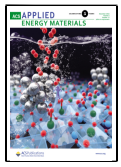

ACS Publications © 2022 American Chemical Society

https://doi.org/10.1021/acsaem.2c02747
ACS Appl. Energy Mater. 2022, 5, 15086−15092

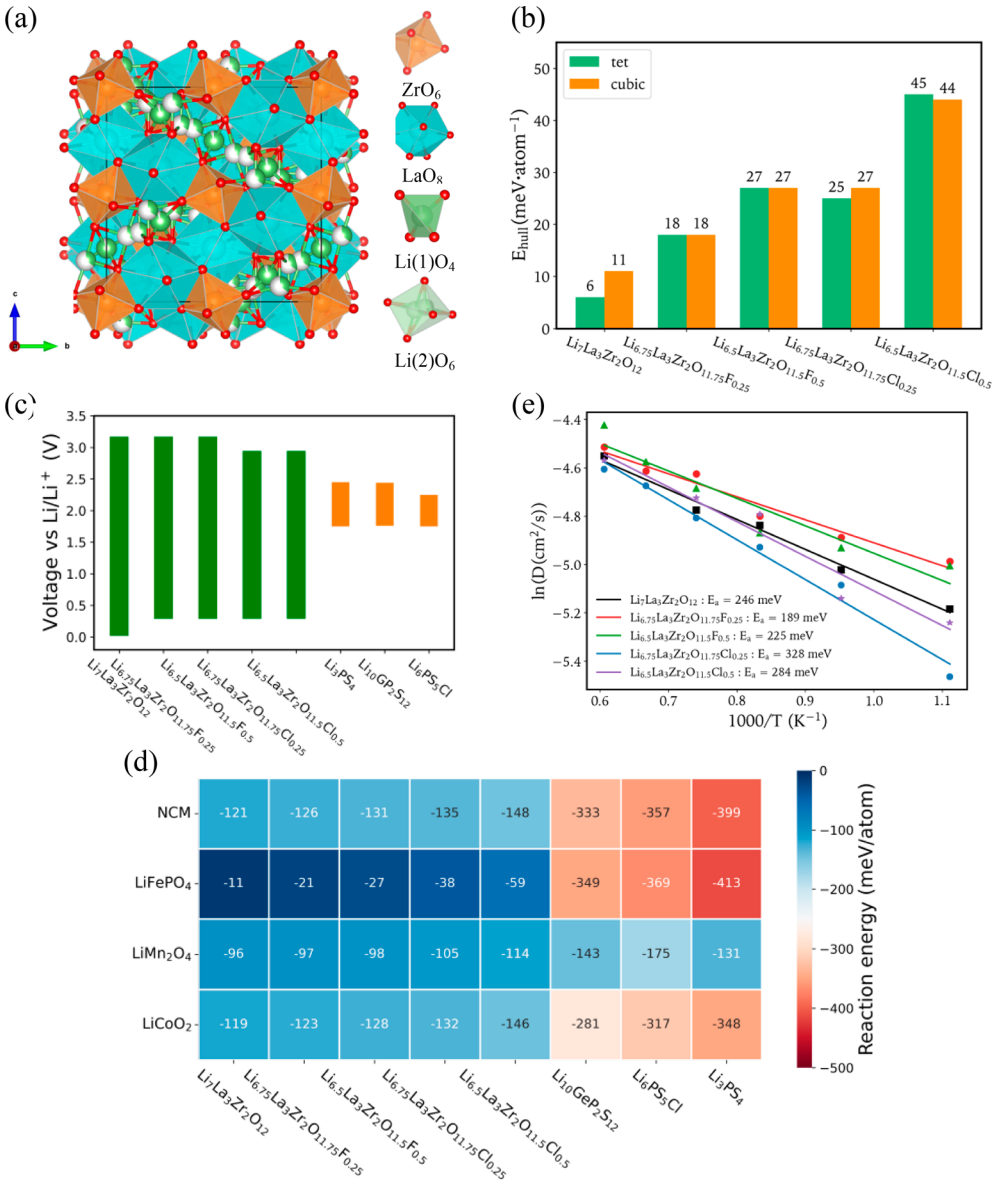

Figure 1. (a) Cubic garnet structure with space group ($Ia\bar{3}d$). The Li1 species are in tetrahedral 24d sites while Li2 species are in octahedral 96h sites. The La (blue) and Zr (red) are coordinated by 8 and 6 oxygens (red), respectively. (b) E_{hull} for $Li_{7-x}La_3Zr_2O_{12-x}M_x$ (M = F, Cl and x = 0, 0.25, 0.5) in cubic and tetragonal phases. (c) Electrochemical stability window of c-$Li_{7-x}La_3Zr_2O_{12-x}M_x$ (M = F, Cl and x = 0, 0.25, 0.5) and lithium sulfide SEs (Li_3PS_4, $Li_{10}GeP_2S_{12}$, and Li_6PS_5Cl). (d) Reaction energy between c-$Li_{7-x}La_3Zr_2O_{12-x}M_x$ (M = F, Cl and x = 0, 0.25, 0.5) and three lithium sulfide SEs and four typical cathodes (LCO, LMO, LFP, and NMC). (e) Arrhenius plot of the Li diffusion coefficient vs temperature of c-$Li_{7-x}La_3Zr_2O_{12-x}M_x$ (M = F, Cl and x = 0, 0.25, 0.5).

($Li_{6.52}La_3Zr_2O_{11.52}F_{0.48}$) system prefers to be cubic at much lower temperatures (~500 K), and the lithium diffusion in these low temperature cubic phases of F-doped LLZO is comparable to that of pure cubic or cation-doped LLZO.[21] However, why F-doped LLZO can exhibit superior ionic conductivity comparable to cation-doped ones and how anion doping affects the complex diffusion mechanisms of Li ions in c-LLZO are still not clear, and atomistic simulations could shed light on this.

In this work, we studied the effects of F and Cl doping in c-LLZO with a Li concentration range of 6.5−7 per formula based on first-principles calculations. The small energy above the hull demonstrates the feasibility of F and Cl doping in c-LLZO. F-doped LLZO has good electrochemical and chemical stability. Ab initio molecular dynamics (AIMD) simulations were performed to investigate the ionic conductivity and activation energy for all the systems considered. Furthermore, Li ion probability density, site occupancy, radial distribution function, time-averaged Li positions, site−site jump events, and phonon density of states were analyzed. It is concluded that the c-LLZO with a homogeneous diffusion network and high Li jump numbers has good ionic conductivity. The introduction of a certain amount of Li vacancies can enhance both the Li jump numbers and the concerted migration percentage of c-LLZO.

■ COMPUTATIONAL METHODOLOGY

Initial Structure Optimization. The c-LLZO was obtained from the ICSD (No. 422259).[22] The 24d Li1 tetragonal site and the 96h Li2 octahedral sites in c-LLZO are partially occupied (see Figure 1a). We obtained the primitive cell for disordered structure and adopted

https://doi.org/10.1021/acsaem.2c02747
ACS Appl. Energy Mater. 2022, 5, 15086−15092

Table 1. Conductivity and Structure Related Properties of c-$Li_{7-x}La_3Zr_2O_{12-x}M_x$ (M = F, Cl and x = 0, 0.25, 0.5)

formula	E_a (meV)	D_0 (cm^2/s)	σ_{300K} (mS/cm)	volume (Å^3)	channel size (Å)
$Li_7La_3Zr_2O_{12}$	246 ± 15	1.50×10^{-4}	1.749	1111.46	1.43
$Li_{6.75}La_3Zr_2O_{11.75}F_{0.25}$	189 ± 18	1.10×10^{-4}	11.233	1111.70	1.47
$Li_{6.5}La_3Zr_2O_{11.5}F_{0.5}$	225 ± 37	1.52×10^{-4}	3.66	1111.93	1.49
$Li_{6.75}La_3Zr_2O_{11.75}Cl_{0.25}$	328 ± 21	2.67×10^{-4}	0.128	1122.75	1.38
$Li_{6.5}La_3Zr_2O_{11.5}Cl_{0.5}$	284 ± 39	2.10×10^{-4}	0.55	1127.50	1.54

site occupancy factors (SOFs) of 0.417 for Li1 and 0.479 for Li2.[23] To prepare initial structures for the simulations, the lithium atoms were arranged based on the SOFs and low electrostatic energy criteria, as implemented in the Python Materials Genomics (pymatgen) analysis code.[24] First, the ions were assigned with the idealized charges, i.e., Li^{1+}, La^{3+}, Zr^{4+}, O^{2-}. Considering a large number of possible permutations of Li positions (>10^{11}), the Li sites were assigned using a simple method of removing the Li sites with the highest electrostatic energy in a sequence until the desired SOFs were reached.[23] For a doped system, first, the dopant was arranged to find the configurations with the lowest electrostatic energy, and then the lithium atoms were further removed due to charge compensation as well as the electrostatic energy criteria. Twenty structures with the lowest electrostatic energy were selected and relaxed with density functional theory (DFT) calculations. The structure with the lowest DFT energy was then chosen for the AIMD simulations.[5] The positions of the doping elements in c-LLZO are shown in Figure S1 in the Supporting Information.

All calculations were performed within the Vienna Ab initio Simulation Package (VASP)[25] software based on the projector augmented wave (PAW) method.[26] The generalized gradient approximation (GGA) with the Perdew−Burke−Ernzerhof (PBE)[27] functional was adopted to consider the electron exchange-correlation energy. In this work, the c-$Li_{7-x}La_3Zr_2O_{12-x}M_x$ primitive cell with M = F and Cl, and x = 0, 0.25, 0.5, was built and relaxed for the subsequent calculations. A plane-wave energy cutoff of 520 eV was used, and the Brillouin zone was sampled by a 2 × 2 × 2 Γ-centered k-mesh. The convergence criteria of the energy and force are 1×10^{-5} eV and 0.01 eV/Å, respectively.

AIMD simulations were performed to evaluate the Li diffusivity with a Γ-centered 1 × 1 × 1 k-point grid, a plane-wave energy cutoff of 300 eV, and non-spin-polarized calculations. The relaxed ground-state structures were heated from 0 K to the desired high temperatures at a constant rate. The time step was set to 2 fs, and all the primitive systems were simulated for 50000 steps with a total time of 100 ps in the NVT ensemble using a Nose−Hoover thermostat.[28,29] For the system with Li vacancy defects, AIMD simulations were performed at 900 K for 50 ps.

Our analysis used the Matplotlib,[30] Pymatgen,[24,31−33] Site-analysis,[34] and Polyhedral-analysis[35] Python packages. The crystal structure plots are displayed by the VESTA software.[36]

■ RESULTS

Phase, Electrochemical, and Chemical Stabilities. The phase stability of a material can be evaluated by constructing the compositional phase diagrams based on the DFT ground-state energies of the corresponding compounds from the Materials Project (MP) database.[37] The E_{hull} of stable phases is 0, and the higher the E_{hull} is, the less stable the phase is predicted to be. Figure 1b shows the E_{hull} for different concentrations of F and Cl in cubic and tetragonal LLZO. Without doping, the E_{hull} value of t-LLZO (6 meV/atom) is smaller than that of c-LLZO (11 meV/atom), which verifies that the tetragonal phase is more stable than the cubic phase at room temperature.[5] The E_{hull} difference between c-LLZO and t-LLZO upon the Cl or F doping decreases or even becomes negative, indicating the cubic phase could be more favored compared to the tetragonal phase. Except for $Li_{6.5}La_3Zr_2O_{11.5}Cl_{0.5}$, all the other compounds are metastable with E_{hull} values below 30 meV/atom, which might be stabilized and synthesized by the entropy effect.[38,39] With the doping concentration increases, the E_{hull} values of both phases increase, indicating that the solubility of F and Cl in c-LLZO is limited.

The electrochemical stability window was calculated based on the grand potential phase diagram as a function of Li chemical potential,[40] as shown in Figure 1c. The calculated stable electrochemical window of the c-LLZO is from 0.03 to 3.17 V. The doping of F had almost no effect on the oxidation potential but slightly increased the reduction potential. The Cl doping systems show a reduced oxidation potential and an increased reduction potential compared to those of c-LLZO. In general, all systems exhibit a wider stability window compared to that of lithium sulfide SE (Li_3PS_4, $Li_{10}GeP_2S_{12}$, and Li_6PS_5Cl). The calculated reaction energy between c-$Li_{7-x}La_3Zr_2O_{12-x}M_x$ (M = F, Cl and x = 0, 0.25, 0.5) and three lithium sulfide SEs and four cathode materials, $Li(NiMnCo)_{1/3}O_2$ (NMC), $LiFePO_4$ (LFP), $LiMn_2O_4$ (LMO), and $LiCoO_2$ (LCO), are demonstrated by the heat map in Figure 4d. The c-LLZO and F doping system exhibits relatively low reaction energies (−27 to −11 meV/atom) against LFP, indicating that the LFP is the most suitable cathode for the systems we studied. The reaction energy between the sulfide SEs and NCM, LMO, and LCO cathode material range from −281 to −413 meV/atom, which would result in chemical decomposition at the interface.

Lithium Ion Diffusivity and Conductivity. The atomic trajectories in Figure S2 show that the anion framework is well maintained and no breaking of bonds was observed during the whole AIMD simulations. Figure 1c shows the Arrhenius plots of the log of the tracer diffusivity, D, versus the reciprocal of the temperature, $1000/T$, for the systems of interest. The c-LLZO has an activation energy of 0.25 eV; this result is close to the AIMD simulation results in Mo's work (0.26 eV).[41] The F-doped systems show a reduced activation energy compared to c-LLZO, while Cl-doping increases the activation energy. The minimum activation energy of 0.19 eV occurs at F = 0.25 per formula.

Table 1 summarizes the extrapolated ionic conductivities at 300 K, $\sigma_{300K,}$ and structure related properties, where the channel size is defined as the largest free sphere diameter that can pass through the structural framework formed by the remaining cations and anions after removing all Li species tructure, analyzed using the Zeo++ software.[42] Compared to intrinsic c-LLZO, the F-doped system shows a slight increase in primitive cell volume (less than 0.05%) and channel size (less than 5%), while the Cl-doped system shows more pronounced changes. However, there is no obvious correlation between volume, channel size, and conductivity. Combined with the radial distribution function of c-LLZOs with and without F or Cl doping at 900 K in Figure S3, it can be seen that all systems have similar Li−O and Li−Li distances (see

https://doi.org/10.1021/acsaem.2c02747
ACS Appl. Energy Mater. 2022, 5, 15086−15092

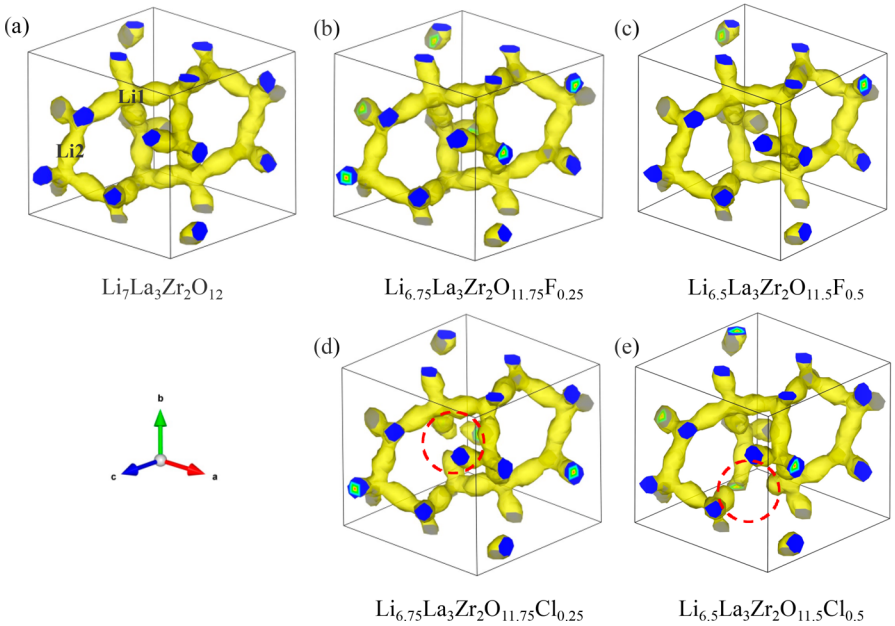

Figure 2. Isosurfaces (yellow) of Li ion probability density distribution for (a) $Li_7La_3Zr_2O_{12}$, (b) $Li_{6.75}La_3Zr_2O_{11.75}F_{0.25}$, (c) $Li_{6.5}La_3Zr_2O_{11.5}F_{0.5}$, (d) $Li_{6.75}La_3Zr_2O_{11.75}Cl_{0.25}$, and (e) $Li_{6.5}La_3Zr_2O_{11.5}Cl_{0.5}$ at 900 K with isovalues is set to 0.002 a_0^{-3} (a_0 is the Bohr radius).

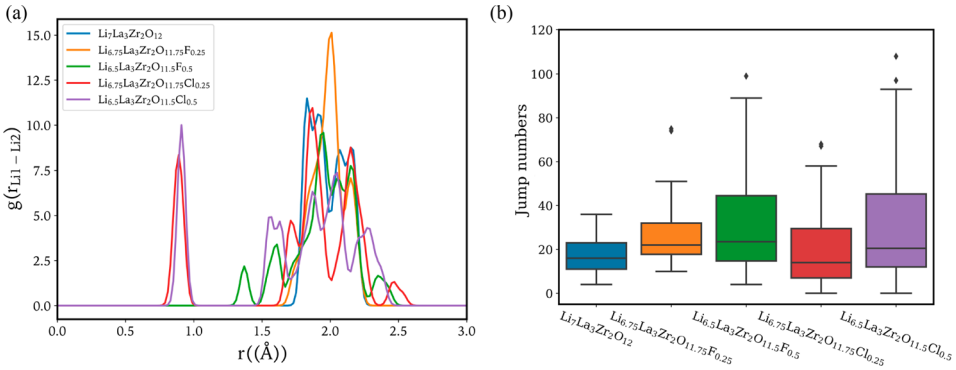

Figure 3. Results from (a) the radial distribution function for time-averaged Li positions for c-$Li_{7-x}La_3Zr_2O_{12-x}M_x$ (M = F, Cl and x = 0, 0.25, 0.5) at 900 K. (b) The boxplot of jump numbers between Li1−Li2 sites for c-$Li_{7-x}La_3Zr_2O_{12-x}M_x$ (M = F, Cl and x = 0, 0.25, 0.5) at 900 K.

Figure S3a,b), Li−F and Li−O distances are almost equal (Figure S3c), and the Li−Cl distance is significantly larger than Li−O distance (Figure S3d). This implies that the effect of F doping on the structure of c-LLZO is very small, mainly in the change of lithium ion concentration, while Cl doping causes local structural distortions, verified by the detailed continuous symmetry measure (CSM) of the lithium polyhedron (shown in Table S1 in SI).[43]

Probability Density and Site Occupancy. Probability density shows the low energy (high probability) Li sites and the migration pathways between them. In c-LLZO, Li ions form a connected diffusion network along the direction of Li1−Li2, with each Li1 connected to four Li2 ions, and each Li2 connected to two Li1 ions, see Figure 2a. The migration paths remain unchanged for the F-doped system compared to intrinsic c-LLZO, but for the Cl-doped system, some migration paths are blocked (in the red circle in Figure 2d,e). These blocked paths may be responsible for the low ionic conductivity of the Cl-doped system.

For c-LLZO, the two adjacent 96h sites in an octahedron cannot be simultaneously occupied. We use the 48g site in the center of the octahedron to define the Li2, and there are 36 available Li sites for the primitive cell (index 0-11 for 24d sites, index 12-35 for 48g sites). We calculated the average Li site occupancies at 900 K,[33,44] as shown in Figure S4. For the Cl-doped system, the Li octahedral site near Cl atoms has a significantly low occupancy (index 25 in Figure S4d and index 12 in Figure S4e), which is due to the weak Li−Cl interaction and the large Li−Cl bond length. These Li octahedral sites with low occupancy correspond to the blocked migration pathways in Figure 2d,e, where the diffusing Li atoms are difficult to access. All systems show lower occupancy at tetrahedral sites than at octahedral sites, in excellent agreement with previous research results.[45]

Time-Averaged Li Positions and Jump Numbers. To obtain more detailed information about how F and Cl doping affects the lithium diffusion, we performed a site-analysis[34] based on the AIMD atomic trajectories. First, each lithium ion is assigned to a specific lithium site (index 0-11 for 24d sites, index 12-35 for 48g sites) at each time step, if the lithium ion is located within the polyhedral volume defined by the instantaneous coordinate of the anions.[46,47] Then, the time-averaged Li positions for a specific site were defined as the average positions of all Li ions that are assigned to that site in

https://doi.org/10.1021/acsaem.2c02747
ACS Appl. Energy Mater. 2022, 5, 15086−15092

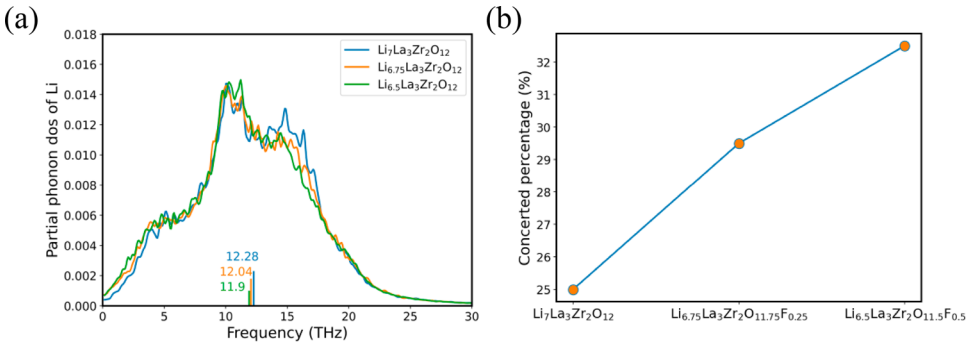

Figure 4. (a) The partial phonon density of states of Li and phonon band centers for c-$Li_{7-x}La_3Zr_2O_{12}$ (x = 0, 0.25, 0.5) at 900 K. (b) Percentage of concerted jumps for c-$Li_{7-x}La_3Zr_2O_{12-x}M_x$ (M = F and x = 0, 0.25, 0.5) at 900 K.

the entire simulation time, reflecting the equilibrium lithium position of the local coordination environment. The radial distribution function for time-averaged Li positions at 900 K is shown Figure 3a. For the Cl-doped system, the peaks show a broader distribution, indicating that there are some polyhedrons with larger distortion and the time-averaged Li positions deviate from the center of the polyhedrons formed by anions. Compared with Cl-doped LLZO, the F-doped LLZO shows a narrower radial distribution peak, indicating a more symmetrical Li polyhedron coordination environment.

The jump numbers represent the number of times the lithium ion moves from one site to a neighboring site. Figure S5 shows the jump number matrices for c-LLZO at 900 K. It can be seen that the jump occurs between each Li1 and its four adjacent Li2 ions and between each Li2 and its two adjacent Li1 ions. The larger the jump numbers are, the more active the diffusion pathway between sites is. We checked the boxplot of jump numbers between Li1−Li2 sites for all systems, as shown in Figure 3b. Compared with the c-LLZO and Cl-doped system, the median values of the jump numbers of the F-doped system are larger, indicating that the mobility of Li ions is enhanced, which is consistent with the larger conductivity of the F-doped system. The Cl-doped system has a larger dispersion (larger interquartile range) in jump numbers, suggesting an inhomogeneous diffusion network, due to large local structural distortions (see Figure 3a). In contrast, the F-doped system has a smaller dispersion in jump numbers, indicating a more homogeneous diffusion network. The same behavior is confirmed for higher simulation temperatures at 1650 K, as shown in Figure S6.

From the above results, it can be concluded that a garnet electrolyte with good ionic conductivity needs to have a homogeneous diffusion network and high Li jump numbers. The homogeneous diffusion network requires that the anion sublattice does not have large local structural distortions leading to inactive diffusion pathways, while a high Li jump number could be related to the Li lattice dynamics, which will be discussed in detail below.

■ DISCUSSION

The Effect of Doping on Li^+ Dynamics. Monovalent anion doping introduces Li vacancies in c-LLZO. To understand how the Li mobility is related to the lithium vacancy concentration, we generated the c-LLZO structure with Li vacancy defects and performed AIMD simulations. The mean square displacement at 900 K is shown in Figure S7, suggesting that the introduction of vacancies improves the diffusivity of the Li ion. In addition, the total jump numbers for the systems with [Li] = 7, 6.75, and 6.5 per formula are 832, 1290, and 1597, respectively, which also indicate the enhanced mobility of Li. Recent work has demonstrated that a lower lithium vibration frequency or lower lithium phonon band center is related to a lower activation energy of fast ionic conductors.[48] Figure 4a shows the partial phonon density of states of Li and phonon band centers at 900 K. The phonon band centers have the relationship $Li_{6.5}La_3Zr_2O_{12}$ < $Li_{6.75}La_3Zr_2O_{12}$ < $Li_7La_3Zr_2O_{12}$, and the phonon mode of Li becomes softer with the introduction of a Li vacancy. The increase in Li jump numbers of c-LLZO containing a Li vacancy may be related to the increase in low frequency (large amplitude) Li vibrations, weakening the interaction between the migrating Li ions and the lattice.[49−51]

It is well-known that there is a multi-ion concerted migration mechanism in c-LLZO that facilitates the reduction of the energy barrier.[52] The plots of the distinct part of the van Hove correlation function at 900 K in Figure S8 show a strong time correlation in Li^+ hopping.[33,52] To quantify the effect of doping on the extent of concerted migration, the jump events were statistically analyzed. The concerted jumps were determined if jumps are correlated in time and space. The time scale for concerted jumps should be on the order of the average atomic vibration, with a value equal to the period of the attempt frequency ($1/\nu^*$ s).[53] The value of the attempts frequency is 1.27×10^{13} Hz, extracted by the code developed by Wagemaker's group,[54] see Figure S9. The spatial condition of the concerted jumps is slightly larger than the largest Li−Li jump distance, set to 3 Å.[55] Due to the large local structural distortion and blocked migration paths of the Cl-doped LLZO, only the c-LLZO and F-doped LLZO were analyzed. Figure 4b shows the ratio of the number of concerted jumps over the total jump numbers, and it can be seen that the percentage of concerted jumps increases with the increase of F concentration. The same trend is demonstrated in the system containing only Li vacancies (Figure S10), implying that concerted jumps occur more frequently when there are more Li vacancies. It is worth noting that the interactions between the lithium ions in c-LLZO are complex, and this is related to the lithium concentration and lithium distribution. For example, Jalem et al. reported there is a concerted migration mechanism with long, multiple-site successive jump events in $Li_5La_3Ta_2O_{12}$ while mainly being limited to single-site successive hopping in $Li_7La_3Zr_2O_{12}$.[56] This difference is attributed to the presence of vacancy dimers in $Li_5La_3Ta_2O_{12}$. Another example is the absence of concerted migration of t-LLZO due to the ordered lithium distribution. Therefore,

https://doi.org/10.1021/acsaem.2c02747
ACS Appl. Energy Mater. 2022, 5, 15086−15092

consideration of the effect of dopants on lithium concentration and lithium distribution is essential to provoke concerted migration of garnet-based solid electrolytes.

The introduction of a certain amount of Li vacancies can enhance both the Li jump numbers and the concerted migration percentage of c-LLZO, which helps to improve the ionic conductivity. However, the ionic conductivity of c-LLZO is also dependent on the homogeneity of the diffusion network. For instance, $Li_{6.5}La_3Zr_2O_{11.5}F_{0.5}$ has a lower ionic conductivity due to a less homogeneous diffusion network compared to $Li_{6.75}La_3Zr_2O_{11.75}F_{0.25}$, although the Li jump numbers and the concerted migration percentage of $Li_{6.5}La_3Zr_2O_{11.5}F_{0.5}$ are higher. Furthermore, the low ionic conductivity of Cl-doped LLZO is also mainly due to the inhomogeneous diffusion network. Thus, the homogeneity of the diffusion network and Li jump numbers (especially the concerted jump numbers) jointly influence the ionic conductivity of c-LLZO.

■ CONCLUSIONS

In summary, The effects of F and Cl doping in c-LLZO were investigated by DFT calculations. The small energy above the hull demonstrates the feasibility of F and Cl doping in c-LLZO. F-doped LLZO has good electrochemical and chemical stability. For c-LLZO, the excellent ionic conductivity depends on high Li jump numbers and a homogeneous diffusion network with less local structural distortion. Li vacancies are beneficial for enhancing the Li mobility and concerted migration percentage in c-LLZO. For the anion doping of c-LLZO, a doping suggestion is to select an ion or ion groups with an ionic radius close to O and unit negative charge, which will not cause large local structural distortion and produce certain Li vacancies. The descriptor of the homogeneity of the diffusion network and Li jump numbers provide general insight into the design of supersonic conductor with isotropic three-dimensional Li diffusion pathways.

■ ASSOCIATED CONTENT

Supporting Information

The Supporting Information is available free of charge at https://pubs.acs.org/doi/10.1021/acsaem.2c02747.

Doped structure, atomic trajectories, radial distribution function, CSM value of the Li octahedron near the doped atom, Li site occupancy, jump number matrices, mean squared displacement, van Hove correlation function, vibration frequency spectrum, and percentage of concerted jumps (PDF)

■ AUTHOR INFORMATION

Corresponding Author

Hong Zhu − *University of Michigan−Shanghai Jiao Tong University Joint Institute, Shanghai Jiao Tong University, Shanghai 200240, China*; orcid.org/0000-0001-7919-5661; Email: hong.zhu@sjtu.edu.cn

Author

Yu Yang − *University of Michigan−Shanghai Jiao Tong University Joint Institute, Shanghai Jiao Tong University, Shanghai 200240, China*

Complete contact information is available at: https://pubs.acs.org/10.1021/acsaem.2c02747

Notes

The authors declare no competing financial interest.

■ REFERENCES

(1) Xu, Z.; Chen, X.; Liu, K.; Chen, R.; Zeng, X.; Zhu, H. Influence of Anion Charge on Li Ion Diffusion in a New Solid-State Electrolyte, Li3LaI6. *Chem. Mater.* **2019**, *31* (18), 7425−7433.

(2) Lu, Z. Computational Discovery of Energy Materials in the Era of Big Data and Machine Learning: A Critical Review. *Materials Reports: Energy* **2021**, *1* (3), 100047.

(3) Jalem, R.; Yamamoto, Y.; Shiiba, H.; Nakayama, M.; Munakata, H.; Kasuga, T.; Kanamura, K. Concerted Migration Mechanism in the Li Ion Dynamics of Garnet-Type $Li_7La_3Zr_2O_{12}$. *Chem. Mater.* **2013**, *25* (3), 425−430.

(4) Xu, M.; Park, M. S.; Lee, J. M.; Kim, T. Y.; Park, Y. S.; Ma, E. Mechanisms of Li + Transport in Garnet-Type Cubic Li 3 + x La 3 M 2 O 12 (M = Te, Nb, Zr). *Phys. Rev. B* **2012**, *85* (5), 052301.

(5) Miara, L. J.; Ong, S. P.; Mo, Y.; Richards, W. D.; Park, Y.; Lee, J.-M.; Lee, H. S.; Ceder, G. Effect of Rb and Ta Doping on the Ionic Conductivity and Stability of the Garnet $Li_{7+2x-y}(La_{3-x}Rb_x)(Zr_{2-y}Ta_y)O_{12}$ ($0 \le x \le 0.375$, $0 \le y \le 1$) Superionic Conductor: A First Principles Investigation. *Chem. Mater.* **2013**, *25* (15), 3048−3055.

(6) Bernstein, N.; Johannes, M. D.; Hoang, K. Origin of the Structural Phase Transition in Li 7 La 3 Zr 2 O 12. *Phys. Rev. Lett.* **2012**, *109* (20), 205702.

(7) Meier, K.; Laino, T.; Curioni, A. Solid-State Electrolytes: Revealing the Mechanisms of Li-Ion Conduction in Tetragonal and Cubic LLZO by First-Principles Calculations. *J. Phys. Chem. C* **2014**, *118* (13), 6668−6679.

(8) Klenk, M.; Lai, W. Local Structure and Dynamics of Lithium Garnet Ionic Conductors: Tetragonal and Cubic Li7La3Zr2O7. *Phys. Chem. Chem. Phys.* **2015**, *17* (14), 8758−8768.

(9) Rettenwander, D.; Redhammer, G.; Preishuber-Pflügl, F.; Cheng, L.; Miara, L.; Wagner, R.; Welzl, A.; Suard, E.; Doeff, M. M.; Wilkening, M.; Fleig, J.; Amthauer, G. Structural and Electrochemical Consequences of Al and Ga Cosubstitution in $Li_7La_3Zr_2O_{12}$ Solid Electrolytes. *Chem. Mater.* **2016**, *28* (7), 2384−2392.

(10) Xu, L.; Li, J.; Deng, W.; Shuai, H.; Li, S.; Xu, Z.; Li, J.; Hou, H.; Peng, H.; Zou, G.; Ji, X. Garnet Solid Electrolyte for Advanced All-Solid-State Li Batteries. *Adv. Energy Mater.* **2021**, *11* (2), 2000648.

(11) Rangasamy, E.; Wolfenstine, J.; Allen, J.; Sakamoto, J. The Effect of 24c-Site (A) Cation Substitution on the Tetragonal-Cubic Phase Transition in Li7-xLa3-xAxZr2O12 Garnet-Based Ceramic Electrolyte. *J. Power Sources* **2013**, *230*, 261−266.

(12) Li, Y.; Wang, C.-A.; Xie, H.; Cheng, J.; Goodenough, J. B. High Lithium Ion Conduction in Garnet-Type Li6La3ZrTaO12. *Electrochem. Commun.* **2011**, *13* (12), 1289−1292.

(13) Deviannapoorani, C.; Dhivya, L.; Ramakumar, S.; Murugan, R. Lithium Ion Transport Properties of High Conductive Tellurium Substituted Li7La3Zr2O12 Cubic Lithium Garnets. *J. Power Sources* **2013**, *240*, 18−25.

(14) Ohta, S.; Kobayashi, T.; Asaoka, T. High Lithium Ionic Conductivity in the Garnet-Type Oxide Li7-X La3(Zr2-X, NbX)O12 (X = 0−2). *J. Power Sources* **2011**, *196* (6), 3342−3345.

(15) Wang, Y.; Richards, W. D.; Ong, S. P.; Miara, L. J.; Kim, J. C.; Mo, Y.; Ceder, G. Design Principles for Solid-State Lithium Superionic Conductors. *NATURE MATERIALS* **2015**, *14*, 1026.

(16) Jalem, R.; Gao, B.; Tian, H.-K.; Tateyama, Y. Theoretical Study on Stability and Ion Transport Property with Halide Doping of Na 3 SbS 4 Electrolyte for All-Solid-State Batteries. *Journal of Materials Chemistry A* **2022**, *10* (5), 2235−2248.

(17) Nam, K.; Chun, H.; Hwang, J.; Han, B. *First-Principles Design of Highly Functional Sulfide Electrolyte of Li10-xSnP2S12-xClx for All Solid-State Li-Ion Battery Applications.* **2020**, *8* (8), 3321−3327.

(18) Patel, S. V.; Banerjee, S.; Liu, H.; Wang, P.; Chien, P.-H.; Feng, X.; Liu, J.; Ong, S. P.; Hu, Y.-Y. Tunable Lithium-Ion Transport in Mixed-Halide Argyrodites $Li_{6-x}PS_{5-x}ClBr_x$: An Unusual Compositional Space. *Chem. Mater.* **2021**, *33* (4), 1435−1443.

(19) Feng, X.; Chien, P.-H.; Patel, S.; Wang, Y.; Hu, Y.-Y. Enhanced Ion Conduction in Li2.5Zn0.25PS4 via Anion Doping. *Chem. Mater.* **2020**, *32* (7), 3036−3042.
(20) Cai, L.; Zhao-Yin, W.; Kun, R. High ion conductivity in garnet-type F-doped $Li_7La_3Zr_2O_{12}$. *J. Inorg. Mater.* **2015**, *30*, 995−1000.
(21) Yeandel, S. R.; Chapman, B. J.; Slater, P. R.; Goddard, P. Structure and Lithium-Ion Dynamics in Fluoride-Doped Cubic $Li_7La_3Zr_2O_{12}$ (LLZO) Garnet for Li Solid-State Battery Applications. *J. Phys. Chem. C* **2018**, *122* (49), 27811−27819.
(22) Adams, S.; Rao, R. P. Ion Transport and Phase Transition in Li7-xLa3(Zr2-xMx)O12 (M = Ta5+, Nb5+, x = 0, 0.25). *J. Mater. Chem.* **2012**, *22* (4), 1426−1434.
(23) Miara, L. J.; Ong, S. P.; Mo, Y.; Richards, W. D.; Park, Y.; Lee, J.-M.; Lee, H. S.; Ceder, G. Effect of Rb and Ta Doping on the Ionic Conductivity and Stability of the Garnet Li7 + 2x-y(La3-XRbx)(Zr2-YTay)O12 ($0 \leq x \leq 0.375$, $0 \leq y \leq 1$) Superionic Conductor: A First Principles Investigation. *Chem. Mater.* **2013**, *25* (15), 3048−3055.
(24) Ong, S. P.; Richards, W. D.; Jain, A.; et al. Python Materials Genomics (pymatgen): A robust, open-source python library for materials analysis. *Computational Materials Science,* **2013**, *68*, 314−319.
(25) Kresse, G.; Furthmüller, J. Efficient Iterative Schemes for *Ab Initio* Total-Energy Calculations Using a Plane-Wave Basis Set. *Phys. Rev. B* **1996**, *54* (16), 11169−11186.
(26) Blöchl, P. E. Projector Augmented-Wave Method. *Phys. Rev. B* **1994**, *50* (24), 17953−17979.
(27) Perdew, J. P.; Burke, K.; Ernzerhof, M. Generalized Gradient Approximation Made Simple. *Phys. Rev. Lett.* **1996**, *77* (18), 3865−3868.
(28) Nosé, S. A Unified Formulation of the Constant Temperature Molecular Dynamics Methods. *J. Chem. Phys.* **1984**, *81* (1), 511−519.
(29) Hoover, W. G. Canonical Dynamics: Equilibrium Phase-Space Distributions. *Phys. Rev. A* **1985**, *31* (3), 1695−1697.
(30) Hunter, J. D. Matplotlib: A 2D Graphics Environment. *Computing in Science & Engineering* **2007**, *9* (03), 90−95.
(31) Mo, Y.; Ong, S. P.; Ceder, G. First Principles Study of the $Li_{10}GeP_2S_{12}$ Lithium Super Ionic Conductor Material. *Chem. Mater.* **2012**, *24* (1), 15−17.
(32) Ong, S. P.; Mo, Y.; Richards, W. D.; Miara, L.; Lee, H. S.; Ceder, G. Phase Stability, Electrochemical Stability and Ionic Conductivity of the $Li_{10\pm1}MP_2X_{12}$ (M = Ge, Si, Sn, Al or P, and X = O, S or Se) Family of Superionic Conductors. *Energy Environ. Sci.* **2013**, *6* (1), 148−156.
(33) Deng, Z.; Zhu, Z.; Chu, I.-H.; Ong, S. P. Data-Driven First-Principles Methods for the Study and Design of Alkali Superionic Conductors. *Chem. Mater.* **2017**, *29* (1), 281−288.
(34) Site-analysis codebase. https://github.com/bjmorgan/site-analysis (accessed Nov 04, 2022).
(35) Polyhedral-analysis codebase. https://github.com/bjmorgan/polyhedral-analysis (accessed Nov 04, 2022).
(36) Momma, K.; Izumi, F. VESTA 3 for Three-Dimensional Visualization of Crystal, Volumetric and Morphology Data. *J. Appl. Crystallogr.* **2011**, *44* (6), 1272−1276.
(37) Jain, A.; Ong, S. P.; Hautier, G.; et al. Commentary: The Materials Project: A materials genome approach to accelerating materials innovation. *APL materials* **2013**, *1* (1), 011002.
(38) Hautier, G.; Jain, A.; Ong, S. P.; Kang, B.; Moore, C.; Doe, R.; Ceder, G. Phosphates as Lithium-Ion Battery Cathodes: An Evaluation Based on High-Throughput Ab Initio Calculations. *Chem. Mater.* **2011**, *23* (15), 3495−3508.
(39) Wang, Y.; Richards, W. D.; Bo, S.-H.; Miara, L. J.; Ceder, G. Computational Prediction and Evaluation of Solid-State Sodium Superionic Conductors Na7P3 × 11 (X = O, S, Se). *Chem. Mater.* **2017**, *29* (17), 7475−7482.
(40) Ong, S. P.; Wang, L.; Kang, B.; Ceder, G. Li-Fe-P-O2 Phase Diagram from First Principles Calculations. *Chem. Mater.* **2008**, *20* (5), 1798−1807.
(41) He, X.; Zhu, Y.; Epstein, A.; Mo, Y. Statistical Variances of Diffusional Properties from Ab Initio Molecular Dynamics Simulations. *npj Computational Materials* **2018**, *4* (1), 1−9.
(42) Willems, T. F.; Rycroft, C. H.; Kazi, M.; Meza, J. C.; Haranczyk, M. Algorithms and Tools for High-Throughput Geometry-Based Analysis of Crystalline Porous Materials. *Microporous Mesoporous Mater.* **2012**, *149* (1), 134−141.
(43) Waroquiers, D.; George, J.; Horton, M.; Schenk, S.; Persson, K. A.; Rignanese, G.-M.; Gonze, X.; Hautier, G. ChemEnv: A Fast and Robust Coordination Environment Identification Tool. *Acta Cryst. B* **2020**, *76* (4), 683−695.
(44) Zhu, Z.; Chu, I.-H.; Deng, Z.; Ong, S. P. Role of Na+ Interstitials and Dopants in Enhancing the Na+ Conductivity of the Cubic Na3PS4 Superionic Conductor. *Chem. Mater.* **2015**, *27* (24), 8318−8325.
(45) Chen, C.; Lu, Z.; Ciucci, F. Data Mining of Molecular Dynamics Data Reveals Li Diffusion Characteristics in Garnet Li7La3Zr2O12. *Sci. Rep* **2017**, *7* (1), 40769.
(46) Morgan, B. J. Mechanistic Origin of Superionic Lithium Diffusion in Anion-Disordered Li6PS5X Argyrodites. *Chem. Mater.* **2021**, *33* (6), 2004−2018.
(47) Huang, H.; Chi, C.; Zhang, J.; Zheng, X.; Wu, Y.; Shen, J.; Wang, X.; Wang, S. Fast Ion Transport Mechanism and Electrochemical Stability of Trivalent Metal Iodide-Based Na Superionic Conductors Na_3XI_6 (X = Sc, Y, La, and In). *ACS Appl. Mater. Interfaces* **2022**, *14* (32), 36864−36874.
(48) Muy, S.; Bachman, J. C.; Giordano, L.; Chang, H.-H.; Abernathy, D. L.; Bansal, D.; Delaire, O.; Hori, S.; Kanno, R.; Maglia, F.; Lupart, S.; Lamp, P.; Shao-Horn, Y. Tuning Mobility and Stability of Lithium Ion Conductors Based on Lattice Dynamics. *Energy Environ. Sci.* **2018**, *11* (4), 850−859.
(49) Jalem, R.; Hayashi, A.; Tsuji, F.; Sakuda, A.; Tateyama, Y. First-Principles Calculation Study of Na+ Superionic Conduction Mechanism in W- and Mo-Doped Na3SbS4 Solid Electrolytes. *Chem. Mater.* **2020**, *32* (19), 8373−8381.
(50) Muy, S.; Schlem, R.; Shao-Horn, Y.; Zeier, W. G. Phonon-Ion Interactions: Designing Ion Mobility Based on Lattice Dynamics. *Adv. Energy Mater.* **2021**, *11* (15), 2002787.
(51) Huang, H.; Wu, H.-H.; Chi, C.; Yang, Y.; Zheng, J.; Huang, B.; Wang, S. Phase-Structure-Dependent Na Ion Transport in Yttrium-Iodide Sodium Superionic Conductor Na 3 YI 6. *Journal of Materials Chemistry A* **2021**, *9* (46), 26256−26265.
(52) He, X.; Zhu, Y.; Mo, Y. Origin of Fast Ion Diffusion in Super-Ionic Conductors. *Nat. Commun.* **2017**, *8* (1), 15893.
(53) Zhang, Z.; Zou, Z.; Kaup, K.; Xiao, R.; Shi, S.; Avdeev, M.; Hu, Y.-S.; Wang, D.; He, B.; Li, H.; Huang, X.; Nazar, L. F.; Chen, L. Correlated Migration Invokes Higher Na+-Ion Conductivity in NaSICON-Type Solid Electrolytes. *Adv. Energy Mater.* **2019**, *9* (42), 1902373.
(54) de Klerk, N. J. J.; van der Maas, E.; Wagemaker, M. Analysis of Diffusion in Solid-State Electrolytes through MD Simulations, Improvement of the Li-Ion Conductivity in β-Li_3PS_4 as an Example. *ACS Appl. Energy Mater.* **2018**, *1* (7), 3230−3242.
(55) de Klerk, N. J. J.; van der Maas, E.; Wagemaker, M. Analysis of Diffusion in Solid-State Electrolytes through MD Simulations, Improvement of the Li-Ion Conductivity in β-Li3PS4 as an Example. *ACS Appl. Energy Mater.* **2018**, *1* (7), 3230−3242.
(56) Jalem, R.; Nakayama, M.; Manalastas, W.; Kilner, J. A.; Grimes, R. W.; Kasuga, T.; Kanamura, K. Insights into the Lithium-Ion Conduction Mechanism of Garnet-Type Cubic $Li_5La_3Ta_2O_{12}$ by Ab-Initio Calculations. *J. Phys. Chem. C* **2015**, *119* (36), 20783−20791.

https://doi.org/10.1021/acsaem.2c02747
ACS Appl. Energy Mater. 2022, 5, 15086−15092